Distinguishing quasiperiodic dynamics from chaos in short-time series

Y. Zou,[1] D. Pazó,[2] M. C. Romano,[3] M. Thiel,[3] and J. Kurths[1]
[1]*Nonlinear Dynamics Group, University of Potsdam, Am Neuen Palais 10, 14469 Potsdam, Germany*
[2]*Instituto de Física de Cantabria, IFCA (CSIC-UC), Avda. Los Castros, 39005 Santander, Spain*
[3]*Department of Physics, University of Aberdeen, Aberdeen AB24 3UE, United Kingdom*
(Received 8 March 2007; published 13 July 2007)

We propose a procedure to distinguish quasiperiodic from chaotic orbits in short-time series, which is based on the recurrence properties in phase space. The histogram of the return times in a recurrence plot is introduced to disclose the recurrence property consisting of only three peaks imposed by Slater's theorem. Noise effects on the statistics are studied. Our approach is demonstrated to be efficient in recognizing regular and chaotic trajectories of a Hamiltonian system with mixed phase space.

DOI: 10.1103/PhysRevE.76.016210 PACS number(s): 05.45.−a, 95.75.Wx, 05.10.−a

I. INTRODUCTION

Recurrence plots (RPs) and the associated recurrence quantification analysis (RQA) have been intensively studied in nonlinear data analysis [1–3]. This technique has been applied to various experimental data sets, ranging from chemistry and physiology to earth sciences and complex synchronization analysis [4–9].

RPs were originally introduced to visualize recurrences of trajectories of dynamical systems in phase space [10]. Suppose we have a dynamical system represented by the trajectory $\{\vec{v}_i\}$ for $i=1,\ldots,N$ in a d-dimensional phase space. We then compute the binary matrix

$$\mathbf{R}_{i,j} = \Theta(\epsilon - \|\vec{v}_i - \vec{v}_j\|), \quad i,j = 1,\ldots,N, \tag{1}$$

where ϵ is a predefined threshold, $\Theta(\cdot)$ is the Heaviside function, and $\|\cdot\|$ is a norm defining the distance between two points. The graphical representation of $\mathbf{R}_{i,j}$, called the "recurrence plot," is obtained by encoding the value "one" by a black point, (i.e., the distance between the respective points is smaller than the predefined threshold ϵ) and "zero" by a white point (i.e., the distance between the respective points is larger than ϵ).

The recurrence time—i.e., the time that the trajectory needs to recur to the neighborhood of a previously visited state—corresponds to a white vertical line in an RP [Fig. 1(a)]. Trivially, for a periodic motion of period T, the states recur at fixed time intervals and, hence, the corresponding RP consists of uninterrupted diagonal lines separated by the distance T [Fig. 1(a)]. The RP of a chaotic system represented in Fig. 1(c) shows far more intricate structures with many interrupted lines. The distance between diagonal lines is then not constant due to the multiple time scales present in the system and the interruption of the lines is due to the exponential divergence of nearby trajectories. The presence of nonperiodic recurrence points is referred to as nontrivial recurrence [11]. Note that in the case of nontrivial recurrences, the trajectory only recurs to the vicinity of the reference point but an exact recurrence cannot be obtained.

Quasiperiodicity is the simplest form of dynamics exhibiting nontrivial recurrence with low complexity. The RP of a uniform quasiperiodic system is shown in Fig. 1(b). In contrast to the periodic case, the distance between the diagonal lines is not constant (indicating different return times). The RP of white noise is rather homogenous, consisting mainly of isolated points, indicating the randomness of the system [Fig. 1(d)]. Comparing Figs. 1(a)–1(d), the RP of quasiperiodic motion has an intermediate complexity.

RPs of quasiperiodic motion exhibit intricate line structures with nonequal distances [Fig. 1(b)], but a complete systematic description of them is still lacking. In this paper, we analyze quasiperiodic dynamics in the context of RPs and discuss the relationship to the rather old, but little-known Slater's theorem [12]. This theorem has recently demonstrated to be a useful and fast tool to determine the existence of shearless tori in (quasi-)Hamiltonian systems [13]. Based on Slater's theorem, we propose a procedure that allows distinguishing quasiperiodic from chaotic dynamics in rather short-time series by means of the RP analysis. In the literature, the power spectrum has been widely used to distinguish quasiperiodicity from chaos. However, for an appropriate estimation of the power spectrum rather long-time series from a stationary regime are necessary, and in many applications only short-time series are available. In this paper, we propose a method which overcomes this difficulty. Furthermore, it can also be applied to multivariate data.

Let us recall that two-frequency quasiperiodic motion densely fills the surface of a torus, which is parametrized by two phase variables with incommensurate (average) frequencies—say, $\omega_1 < \omega_2$. The rotation number γ defined as $\gamma \equiv \frac{\omega_1}{\omega_2}$ is an irrational number. In an RP with $\epsilon > 0$, the white vertical lines between diagonals represent rational approximations of γ because they measure (within a precision ϵ) the common multiples of $T_1 = 2\pi/\omega_1$ and $T_2 = 2\pi/\omega_2$. In other words, for a tolerance of order ϵ, the rationals m/n with the smallest n that approximate γ within that tolerance give rise to black points in the RP. Rational approximations of irrational numbers have a fundamental meaning in number theory, as any irrational number can be approximated arbitrarily closely by rational numbers whose denominators are arbitrarily large [14]. This approximation is captured by the white vertical lines in the RP. Hence, in the following analysis, we mainly focus on these white vertical lines.

This paper is organized as follows. In Sec. II, the histogram of white vertical lines is introduced to link the line structures in an RP to Slater's theorem. In Sec. III, the result is illustrated in the case that the rotation number is the golden mean. In Sec. IV we use the analysis of the recur-

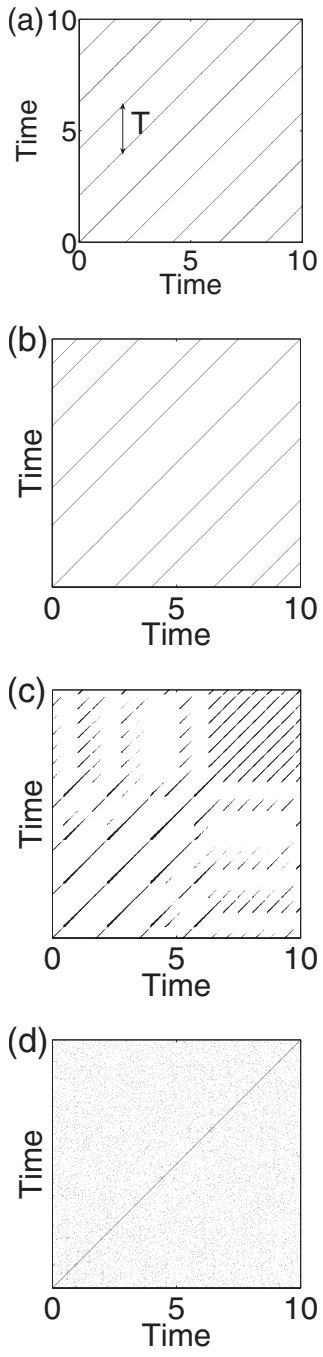

FIG. 1. RPs of four different cases: (a) periodic, (b) quasiperiodic, (c) chaotic, and (d) Gaussian white noise. The line with double arrows in (a) is used to denote a white vertical line.

rence times to distinguish between chaotic and quasiperiodic dynamics in short-time series. The effects of norm type and noise on the return times are studied in Secs. V and VI, respectively. Finally, some conclusions are drawn and discussed in the last section.

II. SLATER'S THEOREM AND LINE STRUCTURES IN THE RPS

We have seen in Fig. 1(b) that the RP of a quasiperiodic trajectory consists of diagonal lines with different distances between them, reflecting the existence of different return times. In this section, we show their relationship to Slater's theorem.

In a three-dimensional phase space, a simple example of quasiperiodic motion, parametrized by time t, is

$$\vec{v}(t) = \begin{pmatrix} x_1 \\ x_2 \\ x_3 \end{pmatrix} = \begin{pmatrix} (R + r\sin\omega_1 t)\cos\omega_2 t \\ r\cos\omega_1 t \\ (R + r\sin\omega_1 t)\sin\omega_2 t \end{pmatrix}, \tag{2}$$

with two angular frequencies ω_1, ω_2 and $R > r$. The frequency ω_1 corresponds to the rate of rotation about the cross section with radius r and period $T_1 = 2\pi/\omega_1$, while the frequency ω_2 corresponds to the large circumference with radius R and period $T_2 = 2\pi/\omega_2$. To illustrate the properties of the RP, the parameters in Eq. (2) are chosen to be $R=4$, $r=0.5$, and $\gamma = (\sqrt{5}-1)/2$. The sampling time is $\Delta t = T_2$, which leads to the points on a Poincaré section perpendicular to the longitudinal direction. The advantage of sampling every T_2 will be illustrated in Sec. V. The length of the time series is 5000 points.

As mentioned before, the rough common period T for the two time scales is given by the time after which the trajectory returns to the ϵ neighborhood of a reference point. Hence, the smaller the value of ϵ is, the better the approximation must be to observe a recurrence. The threshold ϵ determines the length of the white vertical lines in the RP.

The RP of $\vec{v}(t)$, Eqs. (2), and its corresponding histogram of white vertical lines for a fixed value of $\epsilon = 0.2$ are plotted in Figs. 2(a) and 2(b), respectively. We observe that in the histogram of white vertical lines there are only three peaks at $l = 5$, 8, and 13. Moreover, one verifies that these peaks are shifted to smaller values as ϵ is increased, which is clearly seen in Figs. 2(c) and 2(d).

In order to understand the histogram of white vertical lines of the RP for quasiperiodic trajectories [Figs. 2(b) and 2(d)], we briefly recall Slater's theorem [12]. The quasiperiodic dynamics on a 2-torus can be reduced, via a Poincaré section, to an invertible circle map, which is conjugated to the (irrational) linear rotation on a unit circle:

$$F: \theta_{n+1} = \theta_n + \gamma \mod 1. \tag{3}$$

Hence, F is the circle homeomorphism with 0 and 1 being identified. The properties of this linear rotation depend on the arithmetic properties of the rotation number γ. Equation (3) can be analytically derived from Eq. (2) by introducing a Poincaré section perpendicular to the longitudinal direction of the toroidal surface, which can be easily obtained by the sampling rate $\Delta t = T_2$ [15]. Slater's theorem states that for any irrational linear rotation and any connected interval of size ϵ, there are at most three different return times, one of them being the sum of the other two. Two of these three return times are always the consecutive denominators in the continued fraction expansion of the irrational rotation number γ.

Hence, the three return times in the RP of the quasiperiodic trajectory (2) are a consequence of Slater's theorem. As the points of the successive irrational linear iteration are uniformly distributed on the circle, the return times depend only

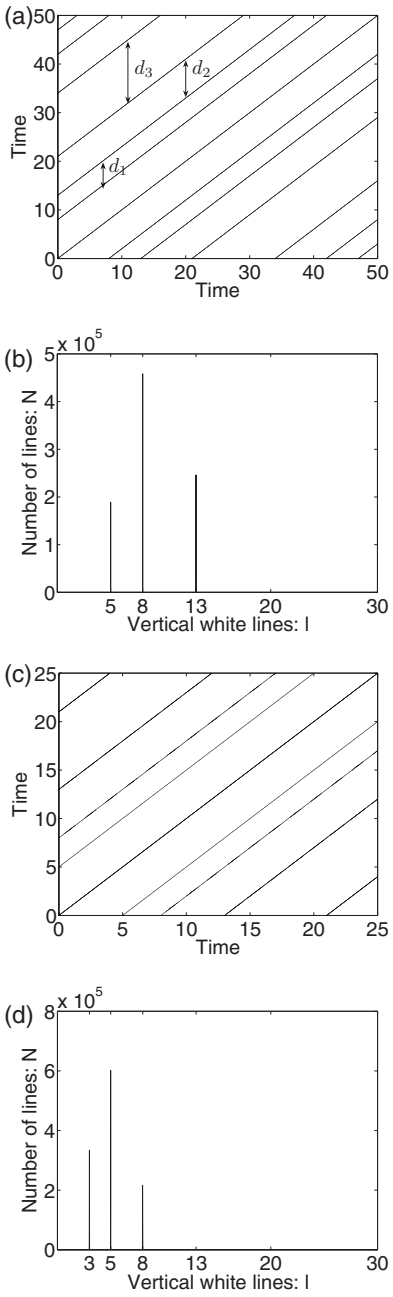

FIG. 2. RPs and the corresponding histograms of the white vertical lines. (a),(b) $\epsilon=0.2$ and (c),(d) $\epsilon=0.3$. The maximal distance is denoted as d_3 in (a).

on the size of the interval. Therefore, the positions of the peaks of the histogram are shifted to larger values as this size is decreased.

However, it is important to note that nonlinearities typically induce nonuniformities in the distribution of the points on the Poincaré section, which automatically implies that intervals of equal length are *not* equivalent (they would become intervals with different lengths under the homeomorphism that allows conjugacy to a rigid rotation by Denjoy's theorem). As a consequence, the return times to intervals of the same size around different reference points are in general not equal; see, e.g., [16–18]. Note that, in particular, the *average* return time for a given interval Δ of a map only

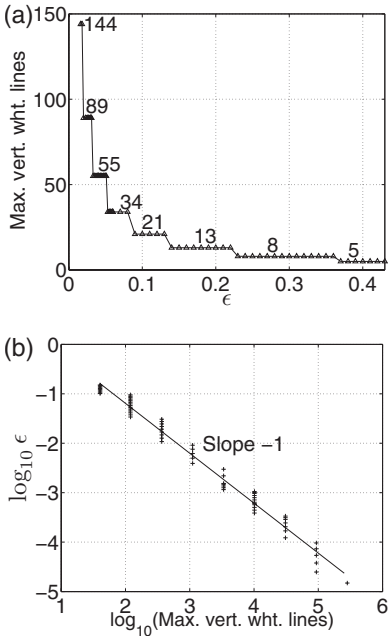

FIG. 3. (a) The maximum white vertical line versus ϵ for the golden mean. The numbers on the plateaus of the curve satisfy the Fibonacci sequence. (b) The ϵ values against the maximal white vertical lines in a logarithmic scale plot. The straight line is with slope −1 as expected by Eq. (7).

depends on the integral $\int_\Delta f(x)dx$, where $f(x)$ is the (smooth) invariant density [17]. This and other subtle aspects of the recurrences are discussed in Sec. V where we study a generic case.

III. EXAMPLE: DYNAMICS WITH THE GOLDEN MEAN AS THE ROTATION NUMBER

We have observed that for uniform quasiperiodic dynamics the white vertical lines in RPs fully reflect the three return times property predicted by Slater's theorem, independently of the position of the reference point. Furthermore, the values of the white vertical lines are determined by the size of the recurrence interval ϵ. In this section, we extend our analysis to explore in more detail the dependence of recurrences (i.e., white vertical lines) on ϵ. We choose the rotation number equal to the golden mean, $\gamma=(\sqrt{5}-1)/2$, as this irrational number has the simplest continued-fraction expansion.

A. Fibonacci sequence

In order to analyze the effect of the size of ϵ on the white vertical lines of the RP, we compute the dependence on ϵ of the largest white vertical line; see Fig. 3(a). We find that the maximal white vertical lines satisfy the Fibonacci sequence $0,1,1,2,3,5,8,13,21,\ldots$, which is defined recursively by

$$F_{n+1}=F_n+F_{n-1}, \quad n=1,2,3,\ldots, \quad \text{and} \quad F_0=0, \quad F_1=1. \tag{4}$$

It is well known that

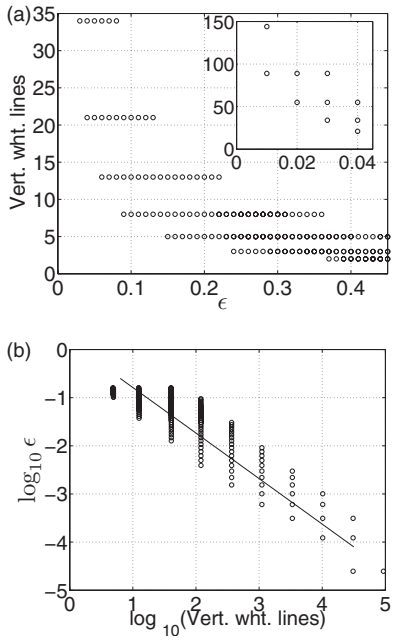

FIG. 4. (a) Three white vertical lines in dependence of ϵ values for the golden mean. (b) The ϵ values against the white vertical lines in a logarithmic plot.

$$\lim_{n\to\infty} \frac{F_{n-1}}{F_n} = \gamma. \tag{5}$$

Instead of plotting only the maximal white vertical line, we now plot in Fig. 4(a) the lengths of *all* the white vertical lines found in the RP. We observe that for each value of ϵ, at most three different lengths of white vertical lines are obtained, in agreement with Slater's theorem. Note that the lengths also satisfy the sum rule, and for this particular rotation number they are proportional to the Fibonacci sequence, with a constant equal to 1 as the time unit is precisely the discrete time of the map (3).

B. Tolerance analysis of the rational approximations

We have seen in the previous sections that, when dealing with quasiperiodic dynamics, the RP reflects the rational approximations to the corresponding frequency ratio of the motion. For practical applications, it is worth discussing and quantifying the degree of approximation and the associated reliability.

According to number theory, an irrational number γ is particularly hard to approximate if it satisfies a Diophantine condition—namely, the inequality

$$\left|\gamma - \frac{m}{n}\right| = |\varepsilon_{(m,n)}| > \frac{C}{n^{\beta+1}}, \tag{6}$$

for some positive numbers $C, \beta \geqslant 1$. It is a basic fact that this set of numbers that are poorly approximated by rationals has Lebesgue measure 1 [19]. In the case of the numbers of constant type, as the quadratic irrationals, $\beta = 1$.

The minimal distance d given by the best rational approximation scales in the following way:

$$d \sim n^{-\beta}. \tag{7}$$

From the RP point of view, this tolerance level d corresponds to the threshold value ϵ for the computation and n corresponds to the length of the white vertical lines in the plot. For the golden mean, a quadratic number we observe the scaling behavior $d \sim n^{-1}$ as expected (see Appendix A). Hence, the relation between the threshold ϵ and the lengths of the white vertical lines in the RP reproduces this scaling behavior, which is seen in log-log scale in Figs. 3(b) and 4(b).

IV. DISTINCTION BETWEEN QUASIPERIODIC AND CHAOTIC DYNAMICS IN SHORT-TIME SERIES

As we have seen in the previous sections, the quasiperiodic dynamics has three return times for a recurrence interval, providing a rather simple technique to detect quasiperiodicity. However, due to the fact that the probabilities of the three respective return times are different from each other as indicated by the value on the y axis in Figs. 2(b) and 2(d), time series with length of more than three orbital periods are required to discard quasiperiodicity. In this section, we apply this property to distinguish quasiperiodic from chaotic orbits in the case that only short-time series are available.

As a case study, we take the Hénon-Heiles Hamiltonian H [20]

$$H = \frac{1}{2}(p_x^2 + p_y^2) + \frac{1}{2}\left(x^2 + y^2 + 2x^2 y - \frac{2}{3}y^3\right), \tag{8}$$

where $p_x \equiv \dot{x}$ and $p_y \equiv \dot{y}$. The corresponding canonical equations read

$$\dot{p_x} = -x - 2xy, \quad \dot{p_y} = -y - x^2 + y^2, \quad \dot{x} = p_x, \quad \dot{y} = p_y. \tag{9}$$

The Hénon-Heiles system was first studied in the context of analyzing the existence of two or three constants of motion in galactic dynamics [20]. Depending on different energy values of the system, it admits a significant number of both regular and chaotic orbits. As the energy increases, the Kolmogorov-Arnold-Moser (KAM) tori begin to dissolve via archipelago formation and the chaotic sea begins to expand. After the last KAM torus has disappeared, a single chaotic component covers almost the entire allowed region of phase space [21]. Throughout this section, we choose an intermediate value of the energy $H = 0.125$, since for this value the regular region has approximately the same size as that of the chaotic one.

A. Visualization: Poincaré map versus RP

Since the system is Hamiltonian, energy conservation imposes trajectories to reside in a three-dimensional volume into the four-dimensional space (x, p_x, y, p_y). It is well known that a proper construction of a Poincaré section allows for an easy visualization of the motion. We define the Poincaré section as $x = 0$, $\dot{x} < 0$. The successive crossings of the trajectories with this section are shown in Fig. 5(a) for ten randomly

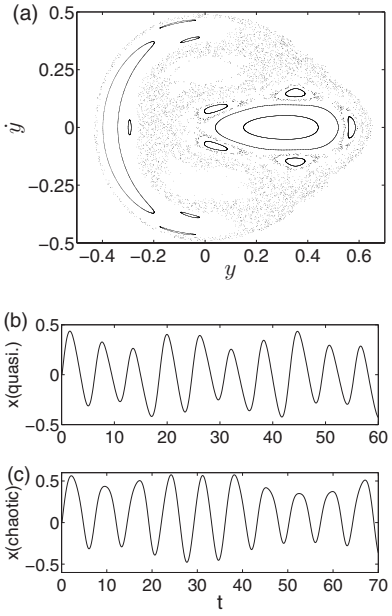

FIG. 5. (a) The crossings of trajectories with the Poincaré section defined by $x=0$, $\dot{x}<0$ for ten random initial conditions for the case with energy $H=0.125$. (b) About ten oscillations of a quasiperiodic orbit with the initial values (0.004 793, 0.479 291, 0.149 994, −0.001 275). (c) A chaotic orbit with the initial conditions (0.004 876, 0.487 553, −0.001 108, −0.110 757).

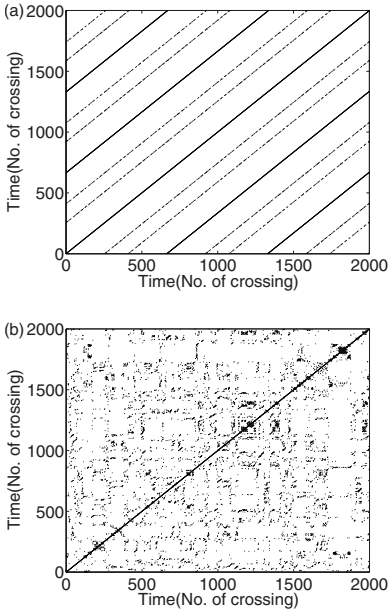

FIG. 6. RPs of the Poincaré section points of two typical trajectories: (a) quasiperiodic and (b) chaotic.

chosen initial conditions. For each trajectory, we terminate the integration of Eqs. (9) when 2000 points on the surface of the section are obtained. The integration is carried out using a fourth-order Runge-Kutta integrator with a fixed step size 0.01 time units The time interval between two consecutive crossings on the section corresponds to the pseudoperiod of one oscillation. The chaotic and quasiperiodic trajectories are identified from Fig. 5(a) as sequences of points in the resulting Poincaré surface of section which, respectively, fill an area and lie on closed smooth curves. This leads to the pictorial notion of a mixed phase space where "islands" of quasiperiodicity surrounding elliptic points are surrounded by the chaotic sea.

The RPs of these 2000 crossings on the Poincaré section are shown in Fig. 6. From this figure, the RP of the quasiperiodic orbit consists of continuous diagonal lines besides regular dashed lines [Fig. 6(a)]. However, the RP of the chaotic orbit has a significantly different line structure [Fig. 6(b)] with many random lines of short length.

In practical applications it may be problematic to define a Poincaré section due to two reasons: first, systems with more than two degrees of freedom might be very difficult to visualize and, second, the dynamical equations may be unknown. Furthermore, if the time series is not very long, the resulting number of points on the Poincaré section might be not enough to conclude whether the successive crossings fall on a closed curve or belong to the chaotic sea. In this case, the RP analysis can distinguish between quasiperiodic and chaotic orbits in a more efficient way.

B. Histogram of white vertical lines in RPs

In order to test the efficiency of RPs with short-time series, we take a quasiperiodic orbit and a chaotic one, of which about ten oscillations are shown in Figs. 5(b) and 5(c). In the following analysis, we try to distinguish between both of them from these ten orbital periods. The results do not depend on the specific initial conditions of the trajectories, and we do not use a Poincaré surface of section either, so we face the problem of analyzing these raw time series without prior knowledge about the Hamiltonian.

First, we present the results in the original space; i.e., we use the trajectories in the four-dimensional (4D) phase space denoted as $(x,\dot{x},y,\dot{y})$ by integrating Eqs. (9) directly. Figures 7(a) and 7(d) show the projections onto the $(x,\dot{x})$ plane of a quasiperiodic and a chaotic orbit, respectively. The associated RPs are generated sampling the trajectory every 0.1 t.u.; see Figs. 7(b) and 7(e). The corresponding histograms of the white vertical lines in RPs are represented in Figs. 7(c) and 7(f), respectively. These histograms allow us to distinguish both cases: only three principal peaks exist for quasiperiodic motion. Furthermore, the length of the largest white vertical line is the sum of the other two. In our particular case, the (sharp) peaks are centered at $T_1=18.45$, $T_2=24.6$, and $T_3=T_1+T_2=43.05$. However, for the chaotic case, there are more than three peaks in the histogram, which noteworthily do not satisfy the very restrictive sum rule of Slater's theorem: for the three principal return times in Fig. 7(f) we have $T_1'=6.7$, $T_2'=35.8$, and $T_3'=49.6$. Note that there are two small peaks at the positions 13.8 and 28.8. Hence, by means of the return times it is possible to distinguish between quasiperiodic and chaotic dynamics from very-short-time series.

We note that in Slater's theorem time is a discrete quantity (like in circle and Poincaré maps); hence, in principle it would be possible to find a system with very low temporal coherence where continuous time and discrete time (from a Poincaré section) are considerably unrelated. We have not encountered this problem, and in turn our histograms always present sharp peaks.

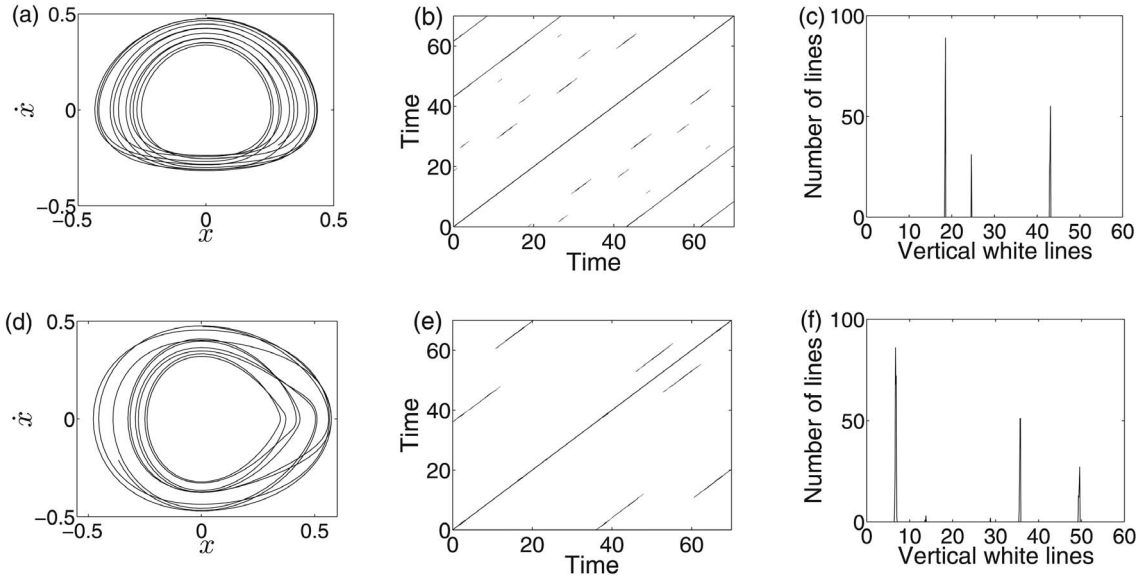

FIG. 7. (a),(d) The projection of the original trajectory in the $(x,\dot{x})$ plane. (b),(e) Recurrence plots. (c),(f) The corresponding histogram of white vertical lines in RPs. The first row (a)–(c) is for the quasiperiodic orbit and the second row (d)–(e) is for the chaotic case.

C. Results with embedded scalar time series

Next, we present the results in the case that only one short *scalar* time series [Figs. 5(b) and 5(c)] is available for the computation of each histogram. The conventional delay embedding is applied before computing the RP. We use an embedding dimension $m=4$ and time delay $\tau=1.7$ t.u., estimated by the autocorrelation function [22]. The projections of the quasiperiodic and chaotic orbits on the $(x,x_{t+\tau})$ plane are shown in Figs. 8(a) and 8(d), which give fairly faithful visual reproductions of the original phase space as Figs. 7(a) and 7(d). After the phase space reconstruction, the RP for each case is shown in Figs. 8(b) and 8(e). The associated histograms of the white vertical lines are plotted in Figs. 8(c) and 8(f), respectively. Based on the histogram of Fig. 8(c) and the relationship between these three peaks $T_1=18.5$, $T_2=24.4$, and $T_3=43\approx T_1+T_2$, one can conclude that the motion is quasiperiodic. However, we get a completely different picture for the chaotic orbit [Fig. 8(f), $T_1'=7$, $T_2'=14$, $T_3'=22$, $T_4'=28.8$, $T_5'=36.1$].

D. Comparison with power spectrum

In the literature, the historically favored method to distinguish quasiperiodic from chaotic orbits is based on the power spectrum. Theoretically, one knows that quasiperiodic trajectories yield discrete Fourier spectra whereas chaotic orbits

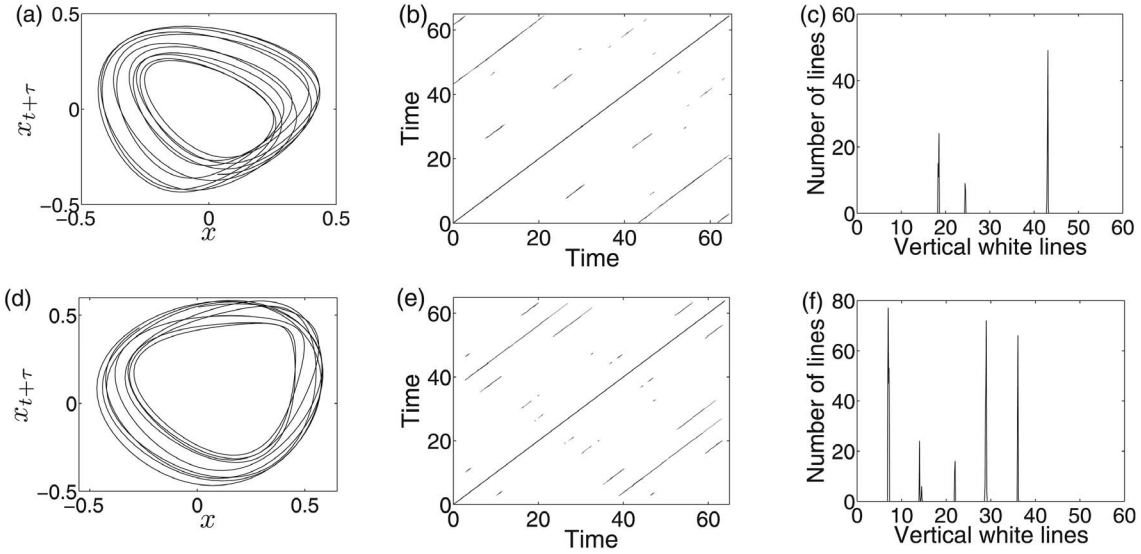

FIG. 8. (a),(d) The projections of the embedded trajectory in the $(x,x_{t+\tau})$ plane. (b),(e) Recurrence plots. (c),(f) The corresponding histogram of white vertical lines in RPs. The first row (a)–(c) is for the quasiperiodic case and the second row (d)–(e) is for the chaotic case.

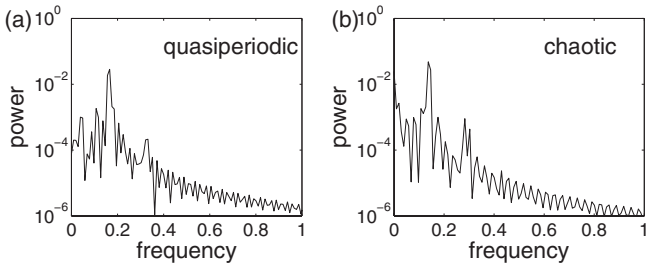

FIG. 9. Power spectra for two cases: (a) quasiperiodic and (b) chaotic. The y axes are in logarithmic scale.

yield continuous (broad) ones. Based on the program "spectrum" of the TISEAN program package [23] the power spectra for our two short-time series (Fig. 9) show that we can hardly come to a significant difference between them. This is due to the rather short-time series used.

Furthermore, the histograms of the white vertical lines in the RPs are constructed from the trajectory in phase space [with four variables $(x,\dot{x},y,\dot{y})$ for example, or $(x,x_{t+\tau},x_{t+2\tau},x_{t+3\tau})$ if it is embedded from the x component], which is an advantage to the conventional power spectrum analysis based on scalar time series. This also prompts the applicability in dealing with multidimensional data analysis. Therefore, the histogram of white vertical lines of the RP contains more information about the dynamics than the power spectrum.

Comparing the histograms and the power spectra, one can infer the existence of quasiperiodicity efficiently from short-time series with the aid of the recurrence properties.

V. NORM EFFECTS ON THE RETURN TIMES

Slater's theorem states that, for any irrational linear rotation on the unit circle, at most three different return times to a connected interval are observed. The application of this theorem to recurrence plots, where one considers recurrences to every point of the trajectory, deserves some caution. Nevertheless, we will see below that considering the recurrences to a fixed point of the trajectory—i.e., using one single column of the RP—this problem can be solved.

First of all, one must differentiate between discrete- and continuous-time systems. If we are able to define a Poincaré section for the system under study, we can apply Slater's theorem directly for the recurrence to a given point, but as we show below, we must take some care for the RP where the recurrences to all points are shown altogether. The case of a continuous-time series is more complicated and encompasses more subtle aspects that we analyze at the end of this section.

A. Circle map model

Once we have a proper Poincaré section of the system under study, we have to choose a norm. In general, due to the lack of uniformity of the motion, intervals with the same length (of the closed curve formed intersecting the torus) are not equivalent. This is something one must always take into account. As nonuniformity is not known in advance, we cannot avoid effects associated with it. In any case, in the ideal case of a *linear* rotation on the unit circle (3), the Euclidean norm is the optimal one. Therefore, as a rule, the Euclidean norm should be the preferred choice for this particular case. Figure 10 exemplifies the goodness of the Euclidean norm versus the maximum norm (that yields recurrence intervals of different length).

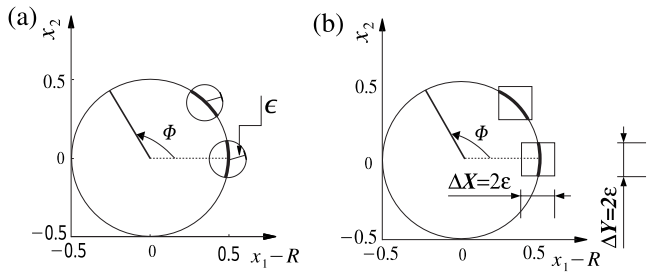

FIG. 10. The effective recurrence interval is denoted by thick arcs. (a) The Euclidean norm yields the same arc length independent of the position due to the symmetry property. (b) The maximum norm yields recurrence intervals of different length due to the invariance of the orientation ΔX in the horizontal (ΔY in the vertical, respectively) direction to the reference point.

In order to show the effect of the maximum norm more clearly, we plot the lengths of the white vertical lines in the RP [using the third component x_3=const of the vector $\vec{v}$ of Eq. (2) as the Poincaré surface] with respect to the position on the circle. The value of the threshold ϵ is the same as used in Fig. 2(b) for better comparison. For illustration, we define a phase variable—say, $\Phi=\arctan x_2/(x_1-R)$—to denote the specific position on the circle.

If the Euclidean norm is used, the return times depend only on the size of the recurrence interval and the number of different recurrence times is 3 [Fig. 11(a)]. In contrast, for the maximum norm, Fig. 11(b) shows that for every refer-

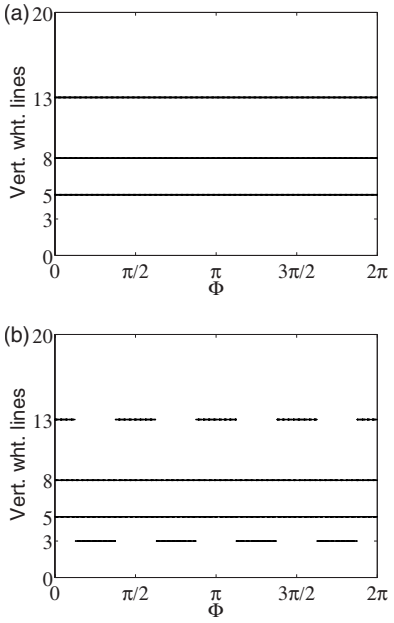

FIG. 11. White vertical lines versus the position on the Poincaré section. (a) The Euclidean norm and (b) the maximum norm.

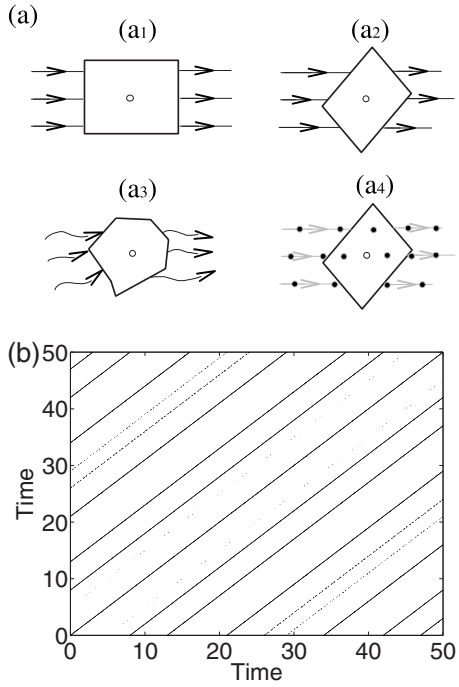

FIG. 12. (a) Schematic description of the relationship between the flow and the recurrence regime on the Poincaré section. The lines with arrows indicate the direction of the flow showing different ways to pass the area. The central circle is the reference point. (a_4) shows the effect of the sampling denoted by black points. (b) RP of quasiperiodic trajectory obtained from Eq. (2). The maximum norm and a sampling time $\Delta t=0.01$ are used.

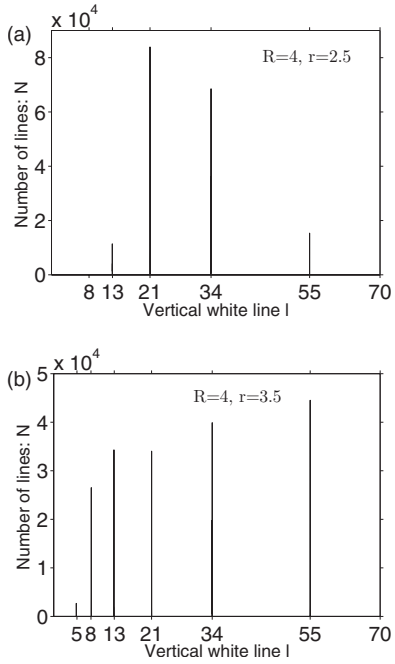

FIG. 13. Histograms of the white vertical lines of the RPs of Eqs. (2) with $R=4$ but for two different values of the radius: (a) $r=2.5$ and (b) $r=3.5$ ($\epsilon=0.25$ in both cases).

ence point, only three different return times are observed. However, the values of these return times vary with the position on the circle. For example, for $\Phi=\frac{\pi}{4}$, the return times are 3, 5, and 8, but for $\Phi=2\pi$, the return times are 5, 8, and 13. Hence, if we count all return times in the RP computed with the maximum norm, we obtain four instead of three recurrence times.

B. Three-dimensional phase space model

Let us see now in more detail how Slater's theorem relates to RPs in a generic situation of recognizing a quasiperiodic flow on a torus. For each point the intersection of the recurrence "ball" (of "radius" ϵ) and the torus gives a two-dimensional recurrence region on the torus. Unless the flow is meandering at the scale of the recurrence region, every recurrence region is crossed by the flow in a regular way (locally every trajectory enters and exists the region once). Hence, for every point of the trajectory the recurrence region encloses a connected recurrence interval as required by Slater's theorem.

The first obvious problem that will typically arise studying a continuous flow is the nonequivalence of different points of the trajectory (due to the different size, orientation, etc., of recurrence regions and due to the nonuniformity of the flow). This will lead to different return times for each point, even if all of them satisfy separately Slater's theorem (like in Fig. 11). In Fig. 12(a), we illustrate some possible idealized ways for the flow to pass the recurrence regions. Intuitively one expects more than three different white vertical lines in the RP as shown in Fig. 12(b), where the maximum is used and the sampling time $\Delta t=0.01$ t.u. in system (2).

Another possible problem that could arise has to do with the measure of the continuous time. As Slater's theorem applies to a discrete-time model, the validity of its extension to a continuous case could be hampered by an extremely poor time coherency. Anyway, we do not expect this will be a serious problem in most applications, as above with the Hénon-Heiles system.

The third unavoidable problem is due to the finite sampling time (see [24] for a recent study of this problem). As shown in Fig. 12(a_4), some recurrences may be skipped if the sampled trajectory jumps over the recurrence region, which would result in an apparent violation of Slater's theorem. This last reason is related to the shape of the torus, which for instance is linked to the values of two radii R and r in Eq. (2). The degree of curvature of the torus determines in how the trajectory enters in the recurrence region. The histograms of the white vertical lines for two different radii $r=2.5$ and 3.5 with the same $R=4$ are shown in Fig. 13 for long trajectories, presenting more than three principal peaks in both cases.

From the above analysis, we see that the norm can affect the statistics of the genuine recurrence property of quasiperiodic dynamics, although these coordinate representations are dynamically equivalent. This could be also one reason why the estimation of the correlation entropy K_2 from time series from a quasiperiodic fluid flow data is larger than zero [25]. For a practical investigation, we should not restrict ourselves to a particular norm, since the norm effects cannot be elimi-

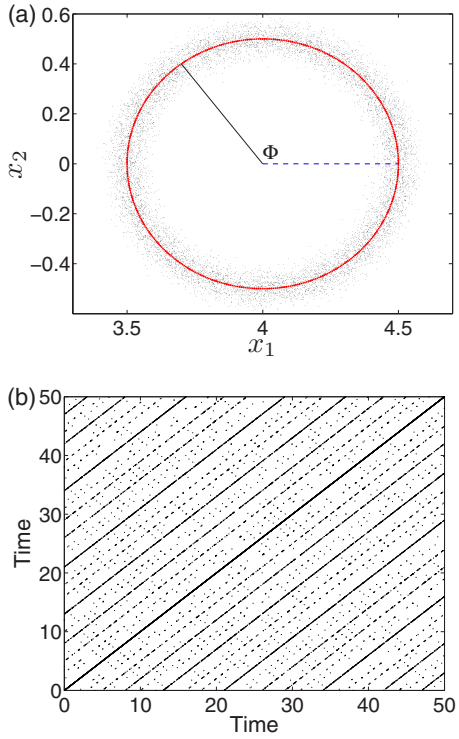

FIG. 14. (Color online) (a) Poincaré section of Eq. (2), x_3 =const, corrupted by 10% of independent Gaussian noise. The original circle is marked by red color. The phase variable Φ is defined as $\arctan x_2/(x_1-R)$. (b) RP with $\epsilon=0.2$. Compared to Fig. 2(a), the continuous lines are broken, leading to subdistances.

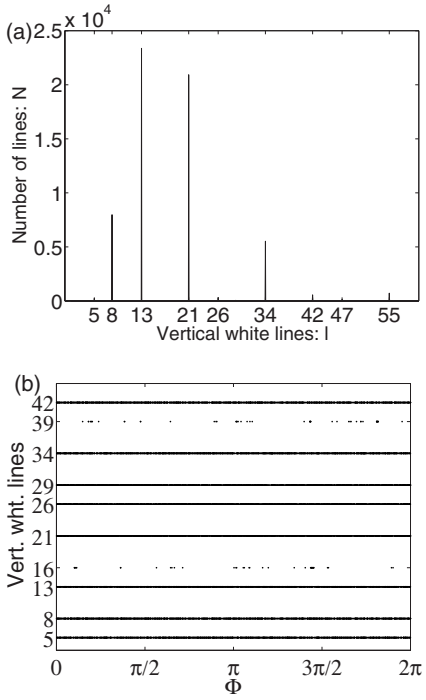

FIG. 15. (a) Histogram of white vertical lines in the RP based on the Poincaré section points of Eq. (2) corrupted by 10% of noise. (b) The return times as a function of the position on the Poincaré section.

nated completely. Instead, we can test the statistics for different norms to minimize the effects of the coordinates to obtain a reliable result.

As we have mentioned above, we can avoid the norm effects by considering recurrences to a fixed point of the trajectory—i.e., considering one single column of the RP. In this case, we will obtain the three return times predicted by Slater's theorem. If, on the other hand, we do want to average the return times over *all* points of the trajectory, we could make use of the dashed structures found in the RPs of quasiperiodic dynamics [Fig. 12(b)]. This structure seems to be characteristic of quasiperiodic dynamics and needs further investigation.

VI. NOISE EFFECTS ON THE RETURN TIMES

In experimental time series, one is always confronted with measurement errors. Hence, it is necessary to analyze the influence of noise on the return times for quasiperiodic motion.

Here, we study the influence of additive (i.e., observational) noise. We generate a time series with a fixed sampling $\Delta t=T_2$ of the system (2) with rotation number equal to the golden mean. We add independent Gaussian noise with standard deviation $\sigma_{noise}=\alpha\sigma_j$ to each coordinate x_j of the crossings on the Poincaré section, where σ_j is the standard deviation of the jth component and $\alpha=0.1$ is the noise level. In Fig. 14(a), the "corrupted" points on the Poincaré surface (x_1-x_2) are represented, and the corresponding RP is illustrated in Fig. 14(b).

We already know that in the histogram of white vertical lines only three peaks should be observed [Fig. 2(b)]. In the case that the trajectory is corrupted by 10% of noise, the continuous lines are broken into small pieces. The probability to find only three return times decreases and some other return times appear [e.g., 34 in Fig. 15(a)]. Figure 15(b) shows the return times as a function of the position of the circle.

From Fig. 14, we see that the line structures are significantly changed. As a consequence, the number of return times is susceptible to observational noise. However, a threshold ϵ that is at least 5 times the standard deviation of the observational Gaussian noise σ can yield reliable statistics [26]. This criterion is based on the analytical computation of the probability of a recurrence point in the RP to be correctly recognized in the presence of observational noise. In [26] it has been found that the choice $\epsilon\sim 5\sigma$ is optimal for a wide class of processes. Based on the suggestion of that finding in [26], choosing ϵ approximately 5 times the standard deviation of the noise, the effects of noise hampering the detection of quasiperiodicity are reduced, as shown in Fig. 16(a). In this diagram, we count the number of return times in the RPs versus ϵ/σ for six different noise levels σ. From Fig. 16(a), we see that the optimized $\epsilon_{opt}\approx 5\sigma$ can be used to recover the three return times to a large extent if there is noise. This recovery is rather good since one often finds three or four values if ϵ_{opt} is applied. Furthermore, the sum relationship between them still holds. A theoretical argument for the choice of the optimized ϵ_{opt} is given in [26].

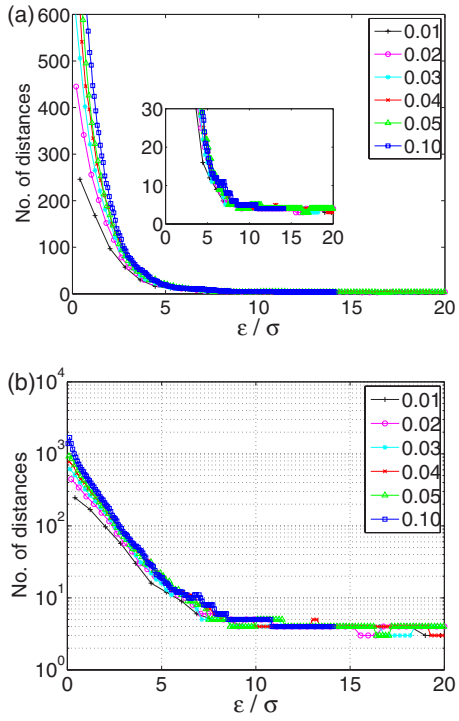

FIG. 16. (Color online) Quasiperiodic trajectory with observational noise for six different levels. (a) The number of white vertical lines versus ϵ/σ. The noise/signal level is given in the legend value. A close look at smaller values is shown in the inset. (b) The same plot of (a) with the y axis in logarithmic scale.

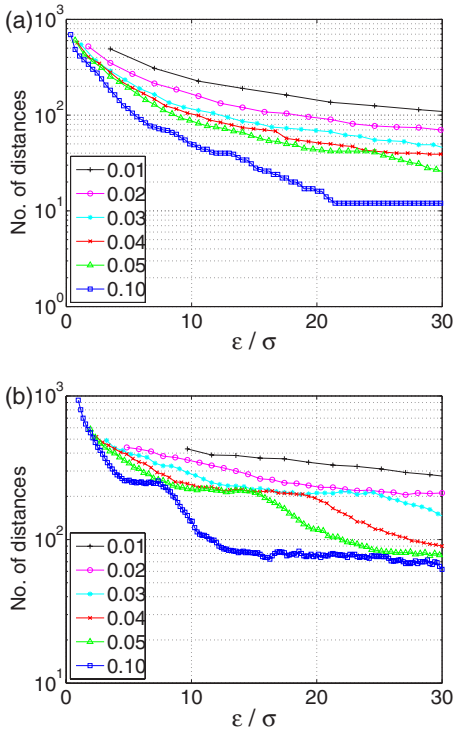

FIG. 17. (Color online) The number of white vertical lines versus ϵ/σ for two chaotic systems with observational noise for six different levels. The y axes are in logarithmic scale and the noise/signal ratio is given in the legend. (a) The Bernoulli map and (b) the Rössler system.

To illustrate the robustness of our procedure to the observational noise we compare the quasiperiodic case with the chaotic one. Hence, we apply the same analysis to two prototypical chaotic systems in the presence of additive noise: namely, the Bernoulli map $f(x)=2x \pmod 1$ on the unit interval and the Rössler system $\dot{x}=-y-z$, $\dot{y}=x+0.2y$, $\dot{z}=0.2+(x-5.7)z$. In the former case the noise is applied only in the x direction, whereas in the latter case the noise enters along the two directions of the Poincaré surface of section. We study the influence of the noise with standard deviation, $\sigma_{noise}=\alpha\sigma_j$, to each coordinate for these two systems, as we have done for the quasiperiodic case (Fig. 17). Comparing this figure to Fig. 16(b), we can distinguish between chaos and quasiperiodic motion in the presence of noise if we choose an appropriate ϵ. For $\epsilon/\sigma \approx 5$, in the case of the quasiperiodic motion, we obtain three or four return times as we discussed above, whereas for the chaotic cases, for similar values of ϵ/σ the number of return times is much larger. We stress that the sum relationship between different return times does not hold anymore if the dynamics is chaotic.

Note that the numerical results presented in this section are based on the crossings on the Poincaré section. As stated before, for many practical applications, a proper Poincaré section is seldom available. We will study noise effects on more realistic situations systematically in a forthcoming paper.

VII. SUMMARY AND DISCUSSION

We have studied the recurrence properties of quasiperiodic dynamics by means of recurrence plots. Despite the simplicity of the dynamics, the line structures of RPs turn out to be quite intricate and display a rich behavior. The analysis has been performed for uniform and nonuniform quasiperiodic motion. We have exemplified our results for the case that the rotation number is the golden mean and the silver mean as well (see Appendix B). The histogram of white vertical lines in an RP successfully captures the recurrence properties, having at most three different return times in the most favorable case.

In general situations, where one analyzes a continuous-time series from a system with very nonuniform dynamics, more than three vertical line lengths may be observed but they have to fit the very restrictive sum rule imposed by Slater's theorem. This allows one to discard the existence of quasiperiodicity in very-short-time series once the sum relation is not fulfilled. To guarantee the existence of quasiperiodicity one would need longer-time series, because (Hamiltonian) chaos may exhibit seemingly quasiperiodic motion for some time if one observes confined chaos or the system is under the stickiness effect. Our approach has several advantages with respect to the conventional techniques: e.g., the power spectrum. Furthermore, it is robust against observational noise if the proper choice of a recurrence interval ϵ being 5 times the standard deviation of noise is taken.

Besides the application in the Hénon-Heiles system, the procedure proposed in this paper might also be of relevance for the study of engineering problems, such as the long-term behavior of underwater sound propagation in the framework of ray chaos theory, where quasiperiodic dynamics consti-

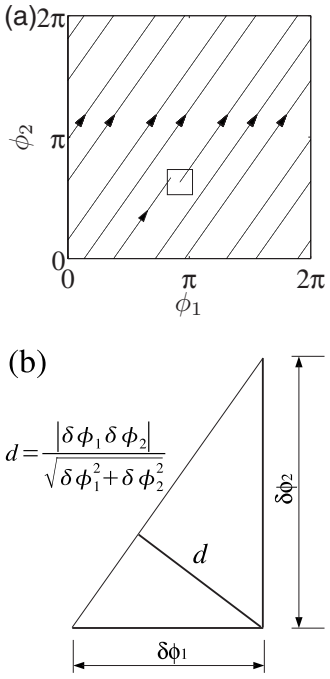

FIG. 18. (a) A short piece of a trajectory on the torus (ϕ_1, ϕ_2). (b) Schematic illustration for the relationship between two errors.

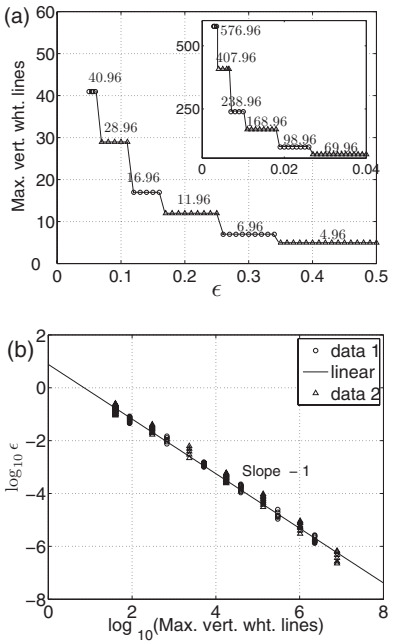

FIG. 19. (a) The maximal vertical distances versus ϵ for the silver mean. The Pell numbers are denoted by △, while ◦ for the Farey neighbors of the Pell numbers. The inset shows the sequence when the ϵ is less than 0.04. (b) Double-logarithmic plot of (a).

tutes the regular region in the phase space [27]. Another particular interesting problem, which could be analyzed by our approach, is the investigation of the transition to chaos via the Takens-Ruelle-Newhouse route, which is closely related to the occurrence of weak turbulence in fluid dynamics [28,29]. Applications to these more complex systems will be addressed in future work.

ACKNOWLEDGMENTS

This work was supported by the International Helmholtz Institute for Supercomputational Physics (MWFK Land Brandenburg), SPP 1114 (DFG), and the Promotionskolleg Behavioral and Cognitive Dynamics (Excellence Programme, Potsdam University). D.P. acknowledges support by Ministerio de Educación y Cultura (Spain) through the Juan de la Cierva Programme and Grants Nos. BFM2003-07749-C05-03 and FIS2006-12253-C06-04.

APPENDIX A: SCALING BEHAVIOR OF THE TOLERANCE ANALYSIS

The tolerance analysis in this section is based on the rational approximation (by continued fractions) to a given irrational rotation number. For convenience, we consider a linear rotation $[\phi_{1,2}(t)=\omega_{1,2}t]$, as shown in Fig. 18(a). Both phases have recurrences at times $T_1(m)=2\pi m/\omega_1$ and $T_2(n)=2\pi n/\omega_2$, which are almost simultaneous $(T_1\approx T_2)$ when $m/n\approx\omega_1/\omega_2=\gamma$. At $T_1(m)$ the recurrence error is given only by the second phase $\delta\phi_2=2\pi m/\gamma$ and, analogously at $T_2(n)$, $\delta\phi_1=2\pi n\gamma$. As illustrated in Fig. 18(b) the minimal distance d is reached at a time T between T_1 and T_2 with

$$d=\frac{|\delta\phi_1\delta\phi_2|}{\sqrt{(\delta\phi_1)^2+(\delta\phi_2)^2}}. \tag{A1}$$

Now, let us denote the distance between an irrational number and a rational one by $\varepsilon_{(m,n)}\equiv\gamma-\frac{m}{n}$. Then we have

$$\delta\phi_1=\gamma 2\pi n=\left(\frac{m}{n}+\varepsilon_{(m,n)}\right)2\pi n=2\pi n\varepsilon_{(m,n)}, \tag{A2}$$

$$\delta\phi_2=2\pi m/\gamma=\left(1-\frac{\varepsilon_{(m,n)}}{\gamma}\right)2\pi n=-2\pi n\frac{\varepsilon_{(m,n)}}{\gamma}. \tag{A3}$$

Substituting Eqs. (A2) and (A3) into Eq. (A1), the minimal distance d satisfies

$$d=2\pi n\frac{|\varepsilon_{(m,n)}|}{\sqrt{1+\gamma^2}}. \tag{A4}$$

If the rational number m/n is a convergent of the continued fraction expansion, then $\frac{C}{n^{\beta+1}}<|\varepsilon_{(m,n)}|<\frac{C'}{n^2}$. In particular, for irrational numbers of constant type, including quadratic irrationals, $\beta=1$, which implies $d\sim n^{-1}$.

APPENDIX B: DYNAMICS WITH THE SILVER MEAN AS THE ROTATION NUMBER

We present here the numerical results for the silver mean $(W^{SM}=\sqrt{2}-1)$ and remark on the similarities and differences with respect to the golden mean case.

First of all we write the sequence of rational approximations to the silver mean: $\frac{1}{2}, \frac{2}{5}, \frac{5}{12}, \frac{12}{29}, \frac{29}{70}, \ldots$. The nth term is given by $W_n^{SM} = G_{n-1}/G_n$, where the G_n are analogous to the Fibonacci numbers and are defined recursively by the Pell sequence

$$G_{n+1} = 2G_n + G_{n-1}, \quad n = 1,2,3, \ldots, \tag{B1}$$

and

$$G_0 = 0, \quad G_1 = 1. \tag{B2}$$

The maximal white vertical lines of the recurrence plots for different values of ϵ are shown in Fig. 19. The results are analogous to Fig. 3; denominators of the continued-fraction expansion appear as required by Slater's theorem, but now they only appear every two plateaus.

[1] J. Zbilut, N. Thomasson, and C. Webber, Med. Eng. Phys. **24**, 53 (2002).
[2] N. Marwan, N. Wessel, U. Meyerfeldt, A. Schirdewan, and J. Kurths, Phys. Rev. E **66**, 026702 (2002).
[3] N. Marwan, M. Romano, M. Thiel, and J. Kurths, Phys. Rep. **438**, 237 (2007).
[4] M. C. Romano, M. Thiel, J. Kurths, I. Z. Kiss, and J. Hudson, Europhys. Lett. **71**, 466 (2005).
[5] J. Kurths, U. Schwarz, C. Sonett, and U. Parlitz, Nonlinear Processes Geophys. **1**, 72 (1994).
[6] M. Thiel, M. Romano, J. Kurths, M. Rolfs, and R. Kliegl, Europhys. Lett. **75**, 535 (2006).
[7] N. Thomasson, T. J. Hoeppner, C. L. Webber, Jr., and J. P. Zbilut, Phys. Lett. A **279**, 94 (2001).
[8] Z.-B. Wu, Phys. Lett. A **332**, 250 (2004).
[9] H. Castellini and L. Romanelli, Physica A **342**, 301 (2004).
[10] J.-P. Eckmann, S. Kamphorst, and D. Ruelle, Europhys. Lett. **4**, 973 (1987).
[11] A. Katok and B. Hasselblatt, *Introduction to the Modern Theory of Dynamical Systems* (Cambridge University Press, Cambridge, England, 1995).
[12] N. Slater, Proc. Cambridge Philos. Soc. **63**, 1115 (1967).
[13] E. G. Altmann, G. Cristadoro, and D. Pazó, Phys. Rev. E **73**, 056201 (2006).
[14] G. Hardy and E. Wright, *An Introduction on the Theory of Numbers*, 3rd ed. (Oxford University Press, Oxford, 1954).
[15] Y. Zou, M. Thiel, M. Romano, and J. Kurths, Int. J. Bifurcation Chaos Appl. Sci. Eng. (to be published).
[16] D. Mayer, Lett. Math. Phys. **16**, 139 (1988).
[17] M. Theunissen, C. Nicolis, and G. Nicolis, J. Stat. Phys. **94**, 437 (1999).
[18] N. Buric, A. Rampioni, and G. Turchetti, Chaos, Solitons Fractals **23**, 1829 (2005).
[19] J. Meiss, Rev. Mod. Phys. **64**, 795 (1992).
[20] M. Hénon and C. Heiles, Astron. J. **69**, 73 (1964).
[21] A. Lichtenberg and M. Lieberman, *Regular and Chaotic Dynamics*, 2nd ed. (Springer, Berlin, 1992).
[22] H. Abarbanel, R. Brown, J. Sidorowich, and L. Tsimring, Rev. Mod. Phys. **65**, 1331 (1993).
[23] R. Hegger, H. Kantz, and T. Schreiber, Chaos **9**, 413 (1999).
[24] A. Facchini and H. Kantz, Phys. Rev. E **75**, 036215 (2007).
[25] M. Thiel, M. Romano, P. Read, and J. Kurths, Chaos **14**, 234 (2004).
[26] M. Thiel, M. Romano, J. Kurths, R. Meucci, E. Allaria, and F. Arecchi, Physica D **171**, 138 (2002).
[27] T. Bodai, A. Fenwick, and M. Wiercigroch (unpublished).
[28] S. Newhouse, D. Ruelle, and F. Takens, Commun. Math. Phys. **64**, 35 (1978).
[29] P. Read, Surv. Geophys. **22**, 265 (2001).